The avidin-theophylline complex: a structural and computational study

Angelo Spinello[a], Fabio Lapenta[b] and Matteo De March[b*]

[a] Department of Biological, Chemical and Pharmaceutical Sciences and Technologies, University of Palermo, 90133 Palermo, IT

[b] Department of Environmental and Biological Sciences, University of Nova Gorica, SI-5000 Nova Gorica, SLO

* Correspondence

Matteo De March: matteo.demarch@ung.si

Abstract

The interaction between avidin and its counterpart biotin is one of central importance in biology and has been repurposed and studied at length. The binding pocket of avidin is however prone to promiscuous binding able to accommodate even non-biotinylated ligands. Comprehending the factors that distinguish the extremely strong interaction with biotin to other ligands is an important step to fully picture the thermodynamics of these low-affinity complexes. Here, we present the complex between chicken white egg avidin and theophylline (TEP), the xanthine derivative used in the therapy of asthma. In the crystal structure, TEP lies in the biotin binding pocket with the same orientation and planarity of the aromatic ring of 8-oxodeoxyguanosine. Indeed, its affinity for avidin measured by Isothermal Titration Calorimetry is in the same μM range as those obtained for the previously characterized nucleoside derivatives. By the use of Molecular Dynamic simulations, we have investigated the most important intermolecular interactions occurring in the avidin-TEP binding pocket and compared with those obtained for the avidin 8-oxodeoxyguanosine and avidin-biotin complexes. These results testify the capability of avidin to complex purely aromatic molecules.

Keywords: crystal structure, binding constant, free-energy, avidin complex, xanthine.

1. Introduction

Avidin is a highly stable tetrameric glycoprotein originally derived from the eggs of aves, reptiles and amphibians. It is composed of four identical subunits with 128 amino acids, each folding into an 8-strand β-barrel. The net positive charge facilitates its binding to negatively charged molecules at physiological pH [1]. Apart from this, avidin is well known due to its extremely strong affinity for biotin (K_d of 10^{-15} M) [2]. Notably, the non-covalent interactions responsible for the avidin-biotin complex are 100 times stronger than those of an antigen-antibody [3], resilient to the change of physicochemical parameters like pH or temperature [4] as well as to the use of denaturing reagents [5]. This extremely high affinity, which makes the formation of the macromolecular complex practically irreversible, can impair experiments that utilizes avidin-biotin system [6]; thus, biotin analogues with weaker and reversible binding, as in the case of desthiobiotin [7], can be used in several applications.

For all these reasons, the avidin-biotin system is constantly used as a versatile module for biochemical and ELISA assays [8-9] and affinity purifications [10]. Few remarkable examples of avidin-biotin repurposed as tool in biomedicine and bio-nanotechnology are the delivery of Kv1.3 siRNAs in the treatment of autoimmune disorders [11] or its usage as cargo for cell penetrating peptides [12]. In addition, avidin-based scaffolds were utilized for Ab functionalisation and vaccine delivery [13-14], imaging and diagnosis of cancer [15-16] and tissue engineering [17]. Furthermore, since biotin is highly expressed in cancer cells [18] avidin can be considered a biological platform for cancer detection.

The presence of a set of aromatics and charged residues in the avidin binding pocket in combination with the chemical characteristics of the biotin itself, *i.e.* a tetrahydrothiophene ring fused to a ureido ring define the strength of this unique and naturally occurring complex [2]. Indeed, over the last decade extensive efforts have been made to develop biotin-based analogues with different affinities to be used in various applications [19-20], but not all of them have been reported as cocrystallizing agents. Up to now, 57 structures of avidin or related avidin are available in the Protein Data Bank (PDB). Many of them are complexed to biotin or biotin-derivates maintaining the well-known geometry and interactions in the binding site: these are biotynilpyrene and its analogues [21], homobiotin and its analogues [22], nitrophenolate [23], ferrocene homobiotin derivative (PDB 5MYQ). A net decreased affinity in the μM range is observed for non-biotin nucleoside derivates, such as 8-oxodeoxyguanosine and 8-oxodeoxyadenosine [24]. Interestingly, in the latter the absence of the C_6-OH completely changes the nucleoside orientation and subsequently the binding interface, yet preserving the affinity [24].

We crystallized avidin in complex with the 1,3-dimethylxanthine TEP. Despite the non-physiological nature of this system, we thought it bears significance for further design of novel avidin-based scaffolds with high affinity for this type of biologically relevant molecules. Furthermore, to uncover the nature of this interaction we characterized it both by Isothermal Titration Calorimetry (ITC) and Molecular Dynamic (MD) simulations.

2. Material and methods

X-Ray structural analysis

Egg white avidin was kindly provided by Prof. F. Berti (University of Trieste) and further dissolved in 50 mM Tris-HCl pH 7.4, 150mM NaCl, 2 mM DTT, 5% glycerol to reach a concentration of 15 mg/mL (0.89 μM). TEP was purchased from Merk (PHR1023, 98%) and dissolved in milliq water with 1% DMSO to reach a concentration of 3.5 μM. To remove the possible presence of contaminants and DMSO the final solution was buffered in 50 mM Tris-HCl pH 7.4, 150mM NaCl, 2 mM DTT using 3MWO amicon filters. The final protein concentration measured at A_{280} was 10.6 mg/mL (0.035 μM).

High throughput crystallization screenings were initially tested using Mosquito (TTP Labtech) obtaining many successful conditions. Single small rood-shaped crystals were tested on X-rays, but only 5% of them reached medium-low resolution (3-4 Å). In most of them the ligand was not present. Final crystals grew by hanging drops in 0.1 M Bis-Tris-propane pH 8.5, 1.7-2.3 M w/v ammonium sulphate, 1-5% v/v MPD after a week at 20 °C. Data were collected at 293 K and wavelength 1.00 on XRD1 beamline (Elettra Sincrotrone) and further processed to 2.2 Å resolution using Mosflm [25] and CCP4i suite [26]. Statistics of data collection and reduction are reported in **Table 1**. Phases were obtained by MR method [27] using PDB 1AVD [28]. Further, the initial model was improved by several cycles of the manual model building using Coot [29] and refinement using REFMAC5 [30]. No jelly-body and NCS restraints were applied [31]. Inspection of the unbiased difference electron density map unambiguously determined the presence of TEP (**Figure 1B**). Solvent molecules were added manually looking to significative hydrogen bonds. Structural analyses were done using CCP4i suite [26]. All figures were prepared with PyMOL [32].

ITC experiments

Egg white avidin was purchased from Sigma-millipore (A9275), resuspended in PBS pH 7.4, filtered and degassed. TEP was prepared following the same procedure. Concentrations were assessed spectrophotometrically, using molar extinction coefficient at 277 nm of 23.615 cm^{-1}

M^{-1} for avidin and of 10.200 cm^{-1} M^{-1} for TEP. The measurements were conducted in triplicate at 25 °C (750 rpm stirring, 150 sec interval) on a MicroCal ITC200 titrating 2 µl of TEP 1.6 mM into a solution of avidin 330 µM. Two consecutive runs, each with 19 injections, were concatenated in the analysis. The bias-free thermogram was integrated with NITPIC [33] and further fit with SEDPHAT [34]. The fitting indicated a large portion of incompetent avidin in the preparation (0.68), which we attributed to the lyophilisation process the sample underwent.

Classical Molecular Dynamics (MD) simulations

We performed classical MD simulations of avidin in complex with TEP, 8-oxodeoxyguanosine (GUA) and biotin (BIO) using a protocol successfully adopted in previous studies [35]. The most likely protonation states under physiological conditions were calculated using the H++ webserver [36]. For the MD simulations we have employed Parm99SB AMBER force field for the protein [37] along with the general Amber FF (GAFF) for the ligands [38]. Electrostatic Potential (ESP) charges were obtained by performing geometry optimization of the compounds at Hartree-Fock level of theory with a 6-31G* basis set using the Gaussian 09 software (*https://gaussian.com/*) and further converted in Restricted Electrostatic potential (RESP) charges using Antechamber module of Ambertools 18 [39]. The resulting three models were solvated using TIP3P water molecules leading to a total of about 90,000 atoms. Finally, the corresponding topologies were built using Ambertools 18 and converted into the GROMACS-compatible format.

Simulations were performed using GROMACS 2020.2 [40] with an integration time step of 2 fs. All covalent bonds involving hydrogen atoms were constrained using the LINCS algorithm. All simulations were done in the NPT ensemble at T 300 K and using a velocity-rescaling thermostat [41]. An initial energy minimization step was performed using the steepest descend algorithm. Models were equilibrated for 20 ns and harmonically restrained using a force constant of 1000 kJ mol^{-1} nm^{-2}. Next, the constraints were gradually released (500, 250, 100 and 50 kJ mol^{-1} nm^{-2}) in four subsequent 20 ns runs, and finally leaving the side chains free of constraint in the last run. Thus, to relax avidin's structure to the presence of the ligand, each system underwent a total of 100 ns-long MD equilibration. Cluster analysis of the MD trajectories was carried out using g_cluster tool. The Amber 18 tool MM_PBSA.py [42] was used to perform Molecular Mechanics Poisson–Boltzmann Surface Area (MM-PBSA) free energy calculation, taking 100 frames from the last 100 ns of the MD trajectories. In particular, a generalized born solvation model was employed (igb=8) [43] using a salt concentration of 0.1 M. The conformational entropic component of the free energy was not considered, since it

was previously suggested that this term does not improve the quality of the results [44]. Visualization of the MD trajectories and preparation of the figures were done using VMD [45].

3. Results & Discussion

Crystal structure of avidin-TEP complex

The structure of the avidin-TEP complex (**Figure 1A**) was solved at 2.2 Å resolution in a new hexagonal form (**Table 1**). Two molecules are present in the asymmetric unit (asu), in agreement with most of the avidin structures previously deposited in the PDB (**Table S1**). The dimer interface is conserved with two monomers facing each other in opposite orientations and symmetric distribution of residues (**Figure S1A**). The combination of transversal intra-chain H-bonds and longitudinal inter-chain interactions stabilizes the entire architecture, as demonstrated for the case of tubulin [46]. The stronger H-bonds are established between Glu74A with Arg59B (3.1 Å), Glu74A with Asn57B (2.8 Å), Glu74A with Thr73B (2.7 Å), Arg100A with Gln82B (2.8 Å), Thr76A with Thr63B (2.8 Å), while important hydrophobic interactions stand between Ile106A and Phe84B (4.1 Å), Leu98A and Leu98B (3.8 Å), Val78A and Val78B (3.6 Å). Being naturally a dimer of dimers, avidin inspired the rational interface engineering of new biomolecular scaffolds with specific mutations favouring or disfavouring the oligomerization process [47]. In the complex with TEP, both monomers are glycosylated at Asn17 and have the ligand present into the binding site (**Figure 1A**). The solvent is constituted by 94 water molecules, one glycerol and 2 sulphate ions. Curiously, they lie at the interface between two monomers A, each of them belonging to different tetramers, thus probably being critical for the formation of the hexagonal packing (**Figure S1B**). The two monomers have a $RMSD_{C\alpha}$ of 0.92 Å and only a difference in the conformation of the T34-E46 loop is evident (**Figure 1A**). This region was already studied [48-49] and reported to be critical for the binding and stability of the ligand [21]. Loop A is completely closed, which results in a more stable binding pocket for TEP. This conformation is critically less prevalent in molecule B due to a crystal contact, as shown by the difference Fo-Fc map (**Figure S1C**). Within this region, T38-S41 residues are highly disordered and cannot be modelled. The presence of the dual loop conformations decreases the binding site rigidity and consequently increases the chances for TEP to be located in different conformations. This was already detected for PDB 5HLM [50], PDB 3FDC [51] and particularly for PDB 4JHQ [52]. The TEP planarity is unambiguously determined into the binding pocket by the unbiased difference Fo-Fc map (**Figure 1B**). Moreover, TEP has a prevalent orientation and forms interactions with Ser16, Tyr33, Trp70, Thr77, Phe79, Trp97, Leu99 and Asn118, conserved in both molecules. When the binding

pocket is closed Thr35 interacts with TEP through its hydroxyl group. On the other hand, when the loop opens, Thr37 stabilizes the β-sheet pushing away this region (**Figure 1B**). The carbonyl group of Val36 confers additional stability to the closed configuration. Notably, TEP overlaps the aromatic ring of 8-oxodeoxyguanosine (PDB 2A5B, [23] (**Figure S1D**). The two binding sites are mainly conserved, but in the latter the nucleoside analogue is stabilized by the interactions made by the sugar group with Phe72, Ser73 and Ser74. Mutations F72E, S73F and S75F would impair more stability even to TEP that has intrinsically more degree of freedom and consequently less affinity.

Avidin has low affinity for TEP

ITC measurements on the avidin-TEP complex (**Figure 2**) showed that the binding constant K_d is 440 μM, in the same μM order to those obtained by fluorescent titration for 8-oxodeoxyguanosine and deoxyguanosine [23]. Compared to its natural ligand this affinity is several orders of magnitude weaker. The thermodynamics of the binding event is characterized by a free energy (ΔG) of -4.813 kcal/Mol, enthalpy (ΔH) of -5.750 kcal/Mol and entropy (ΔS) of -3.142 kcal/Mol. The favourable binding enthalpy is probably due to the chances of TEP to be located in different poses, which facilitate the transition to the crystalline state (**Figure 2B**).

Free-energy of TEP recognition by avidin

To investigate the avidin-TEP complex in solution we have performed 300 ns long MD simulations and obtained a representative pose at the free-energy minimum. For this we have use the avidin dimer as starting model. Not surprisingly, the open conformation of loop B causes the dissociation of TEP after 30 ns from the avidin binding pocket and thus it was excluded from further analyses. Conversely, the closure of loop A stabilizes TEP inducing the unbinding event within 300 ns. This short-timescale is in agreement with the binding constant experimentally measured by ITC. For comparison, we have performed MD simulations on the avidin-GUA and avidin-BIO complexes [53]. The representative poses obtained after cluster analysis are shown in **Figure 3**. Respect to what happened in the crystal structure, TEP assumes in the binding pocket a different position, being its xanthene moiety oriented toward the outer face of the protein making a critical H-bond with Thr38 and a π-π stacking with Trp97 (**Figure 3A**). Similarly, the aromatic part of GUA is stabilized by the interaction with Thr77 and Trp97 in the opposite conformation compared to the one found in the crystal structure [23] (**Figure 3B**). We believe that this difference is due to the dynamics of the loop, limited to only 2 conformations by the crystalline packing and which instead allows in silico to reach the correct

positioning of the TEP on the minimum energy. In both cases the H-bonds with Ser16, Thr33 and Ser75, critical for the binding of biotin (**Figure 3C**), are lost. The more-transient nature of these two structurally similar complexes is highlighted even by the persistent H-bond analysis that shows the stable presence of Thr38 as main interactor with the TEP -O1 group (**Table S2**). It is interesting that GUA remains anchored to the protein by the sugar group but its aromatic ring is more dynamic as the -O3 and -O5 groups, one to the opposite side to the other, interact both persistently with Thr77 (**Table S2**), in accordance with previous findings [23]. **Figure S2** shows the change of the angle made by the aromatic rings of both TEP and GUA within the avidin binding pocket during the whole trajectory in comparison with BIO. Thus, we have better characterized the biophysical properties of the intermolecular interactions within the avidin-TEP and avidin-GUA complexes using Molecular Mechanics Generalized Born Surface Area (MM-GBSA) method [42] and calculated the per-residue decomposition of the binding free energy (ΔG_b) (**Table 2**). Being performed at force field (FF)-level on equally spaced frames extracted from simulation trajectories, this calculation provides insights on the important either non-bonded or hydrophobic and electrostatic interactions between the protein and the ligand. Overall, when compared to the avidin-BIO complex, which exhibits a ΔG of about -22 kcal/mol, the lower binding affinity of about -10 kcal/mol obtained both for TEP and GUA (**Table 2**) is in agreement with their faster dissociation. The aromatic molecule alone implies the reduction of the binding capacity by avidin both in terms of number of interacting residues and binding energy. This is clearly proved by the presence of 7 weak interactions with ΔG_b smaller than -1.0 kcal/mol, in comparison to the avidin-BIO where they are totally absent. This effect is slightly less pronounced in the case of nucleoside analogue most probably by the presence of the sugar moiety. However, the main contribution to TEP stabilization comes from Trp97 with ΔG_b greater than -2.01 kcal/mol, Thr38 and Val37 with ΔG_b between -1.01 and -2.00 kcal/mol. These two interactions are not used by avidin to bind GUA, which instead is prevalently stabilized by Thr77, Leu 99 and Trp70.

4. Conclusions

So far, from the first description of the avidin-biotin interaction in 1940, many biotinylated ligands with diverse chemical derivatizations and consequently modified affinities have been crystallized into the binding site of this protein. To our knowledge, the recognition of TEP by avidin represents a novelty experimentally providing the capability of this very-well know scaffold to bind, albeit with low affinity, even purely aromatic molecules, and thus testifying about the promiscuous nature of its binding pocket. We believe this complex could serve as

platform for the rational design of new avidin mutants with higher affinity and selectivity for – but not limited to – xanthin molecules and be used in biotechnology.

Fundings

This research was conducted with the support of the Slovenian Research Agency ARRS Project Z1-3194 (FL), Regione Autonoma FVG (MDM) and the European Union - NextGenerationEU through the Italian Ministry of University and Research under PNRR - M4C2-I1.3 Project PE_00000019 "HEAL ITALIA" (AS) CUP (B73C22001250006).

Acknowledgments

We thank Prof. S. Geremia (University of Trieste) for FVG grant acquisition and Dr. A. Cassetta (CNR-IC) for access to the ITC.

Author Contributions

ITC data curation and analysis: FL. Crystallographic data curation and analysis: MDM. MD simulations and analysis: AS. Conceptualization: MDM. Investigation: AS, FL and MDM. Manuscript preparation, review and discussion: AS, FL and MDM. All authors have agreed with the published version of the manuscript.

Data Availability Statement

Coordinates and structure factors of the avidin-theophylline complex have been deposited in the Protein Data Bank (PDB, https://www.rcsb.org/) with accession number 8CK7.

Conflicts of interest

Authors declare there are no conflicts of interest.

References

[1] Hama, Y.; Urano, Y.; Koyama, Y.; Kamiya, M.; Bernardo, M.; Paik, R.S.; Krishna, M.C.; Choyke, P.L.; Kobayashi, H. In vivo spectral fluorescence imaging of submillimeter peritoneal cancer implants using a lectin-targeted optical agent. *Neoplasia.* **2006**, 8(7), 607–12.

[2] Rosano, C.; Arosio, P.; Bolognesi, M. The X-ray three-dimensional structure of avidin. *Biomol. Eng.* **1999**, 16(1–4), 5-12.

[3] Ellison, D.; Hinton, J.; Hubbard, S.J.; Beynon, R.J. Limited proteolysis of native proteins: the interaction between avidin and proteinase K. *Protein Sci.* **1995**, 4(7), 1337–1345.

[4] González, M.; Argaraña, C.E.; Fidelio, G.D. Extremely high thermal stability of streptavidin and avidin upon biotin binding. *Biomol Eng.* **1999**, 16, 67-72.

[5] Green, N.M. Avidin.4 Stability at extremes of pH and dissociation into subunits by guanidine hydrochloride. *Biochem. J.* **1964**, 89, 609–620.

[6] Ostrowska, M.; Bartoszewicz, Z.; Bednarczuk, T.; Walczak, K.; Zgliczyński, W.; Glinicki, P. The effect of biotin interference on the results of blood hormone assays. *Endokrynol Pol.* **2019**, 70(1), 102-121.

[7] Huynh, V.; Wylie, R.G. Competitive Affinity Release for Long-Term Delivery of Antibodies from Hydrogels. *Angew Chem Int Ed Engl.* **2018**, 57(13), 3406-3410.

[8] Ahrens, L.; Vonwil, D.; Arya, N.; Forget, A.; Shastri, V.P.; Biotin-Avidin-Mediated Capture of Microspheres on Polymer Fibers. *Molecules.* **2019**, 24(11), 2036.

[9] Shah, M.A.; Ullah, R.; De March, M.; Shah, M.S.; Ismat F.; Habib M.; Iqbal, M.; Onesti, S.; Rahman, M. Overexpression and characterization of the 100K protein of Fowl adenovirus-4 as an antiviral target. *Virus Res.* **2017**, 238, 218-225.

[10] Neimair J.; D'Ercole, C.; De March, M.; Elsner, M.; Seidel, M.; de Marco, A. Macroporous Epoxy-Based Monoliths Functionalized with Anti-CD63 Nanobodies for Effective Isolation of Extracellular Vesicles in Urine. *Int. J. of Mol. Sci.* **2023**, 24, 6131-6144.

[11] Hajdu, P.; Chimote, A.A.; Thompson, T.H.; Koo, Y.; Yun, Y.; Conforti, L. Functionalized liposomes loaded with siRNAs targeting ion channels in effector memory T cells as a potential therapy for autoimmunity. *Biomaterials.* **2013**, 34(38), 10249–10257.

[12] Säälik, P.; Elmquist, A.; Hansen, M.; Padari, K.; Saar, K.; Viht, K.; Langel, U.; Pooga, M. Protein cargo delivery properties of cell-penetrating peptides. A comparative study. *Bioconjug. Chem.* **2004**, 15(6), 1246–1253.

[13] Weir, C.; Hudson, A.L.; Moon, E.; Ross, A.; Alexander, M.; Peters, L.; Langova, V.; Clarke, S.J.; Pavlakis, N.; Davey, R.; Howell, V.M. Streptavidin: a novel immunostimulant for the selection and delivery of autologous and syngeneic tumor vaccines. *Cancer Immunol. Res.* **2014**, 2(5), 469–479.

[14] Pardridge, W.M. Blood–brain barrier drug delivery of IgG fusion proteins with a transferrin receptor monoclonal antibody. *Expert Opin. Drug Deliv.* **2015**, 12(2), 207–222.

[15] Galli, F.; Rapisarda, A.S.; Stabile, H.; Malviya, G.; Manni, I.; Bonanno, E.; Piaggio, G.; Gismondi, A.; Santoni, A.; Signore A. In vivo imaging of natural killer cell trafficking in tumors, *J. Nucl.Med.* **2015**, 56(10), 1575–1580.

[16] Barbet, J.; Bardiès, M.; Bourgeois, M.; Chatal, J.F.; Chérel, M.; Davodeau, F.; Faivre-Chauvet, A.; Gestin, J.F.; Kraeber-Bodéré, F. Radiolabeled antibodies for cancer imaging and therapy. *Methods Mol. Biol.* **2012**, 907, 681–697.

[17] Pan, J.F.; Liu, N.H.; Shu, L.Y.; Sun, H. Application of avidin-biotin technology to improve cell adhesion on nanofibrous matrices. *J. Nanobiotechnol.* **2015**, 13:37.

[18] Bodey, B.; Bodey, B.Jr.; Siegel, S.E.; Kaiser, H.E. Immunocytochemical detection of leukocyte-associated and apoptosis-related antigen expression in childhood brain tumors. *Crit Rev Oncol Hematol.* **2001**, 39(1-2), 3-16.

[19] Dixon, R.W.; Radmer, R.J.; Kuhn, B.; Kollman, P.A.; Yang, J.; Raposo, C.; Wilcox, C.S.; Klumb, L.A.; Stayton, P.S.; Behnke, C.; Le Trong, I.; Stenkamp, R. Theoretical and experimental studies of biotin analogues that bind almost as tightly to streptavidin as biotin. *J Org Chem.* **2002**, 67(6), 1827-37.

[20] Yamamoto, T.; Aoki, K.; Sugiyama, A.; Doi, H.; Kodama, T.; Shimizu, Y.; Kanai, M. Design and synthesis of biotin analogues reversibly binding with streptavidin. *Chem Asian J.* **2015**, 10(4), 1071-8.

[21] Strzelczyk, P.; Plażuk, D.; Zakrzewski, J.; Bujacz, G. Structural Characterization of the Avidin Interactions with Fluorescent Pyrene-Conjugates: 1-Biotinylpyrene and 1-Desthiobiotinylpyrene. *Molecules.* **2016**, 21(10), 1270.

[22] Pazy, Y.; Kulik, T.; Bayer, E.A.; Wilchek, M.; Livnah, O. Ligand exchange between proteins. Exchange of biotin and biotin derivatives between avidin and streptavidin. *J Biol Chem.* **2002**, 277(34), 30892-30900.

[23] Burt, A.J.; Ahmadvand, P.; Opp, L.K.; Ryan, A.T.; Kang, C.; Mancini, R.J. A Ligand-Directed Nitrophenol Carbonate for Transient in situ Bioconjugation and Drug Delivery. *ChemMedChem.* **2020**, 15, 2004-2009.

[24] Conners, R.; Hooley, E.; Clarke, A.R.; Thomas, S.; Brady, R.L. Recognition of oxidatively modified bases within the biotin-binding site of avidin. *J Mol Biol.* **2006**, 357(1), 263-74.

[25] Powell, H.R.; Battye, T.G.G.; Kontogiannis, L.; Johnson, O.; Leslie, A.G.W. Integrating macromolecular X-ray diffraction data with the graphical user interface iMosflm. *Nat Protoc*. **2017**, 12(7), 1310-1325.

[26] Winn, M.D.; Ballard, C.C.; Cowtan, K.D.; Dodson, E.J.; Emsley, P.; Evans, P.R.; Keegan, R.M.; Krissinel, E.B.; Leslie, A.G.; McCoy, A.; McNicholas S.J.; Murshudov, G.N.; Pannu, N.S.; Potterton, E.A.; Powell, H.R.; Read, R.J.; Vagin, A.; Wilson, K.S. Overview of the CCP4 suite and current developments. *Acta Crystallogr D Biol Crystallogr.* **2011**, 67(Pt 4), 235-42.

[27] Vagin, A.; Teplyakov, A. Molecular replacement with MOLREP. *Acta Crystallogr D Biol Crystallogr.* **2010**, 66(Pt 1), 22-5.

[28] Pugliese, L.; Coda, A.; Malcovati, M.; Bolognesi, M. Three-dimensional structure of the tetragonal crystal form of egg-white avidin in its functional complex with biotin at 2.7 A resolution. *J Mol Biol.* **1993**, 231(3), 698-710.

[29] Emsley, P.; Lohkamp, B.; Scott, W.G.; Cowtan, K. Features and development of Coot. *Acta Crystallogr D Biol Crystallogr.* **2010**, 66(Pt 4), 486-501.

[30] Murshudov, G.N.; Vagin, A.A.; Dodson, E.J. Refinement of macromolecular structures by the maximum-likelihood method. *Acta Crystallogr D Biol Crystallogr.* **1997**, 53(Pt 3), 240-55.

[31] De March, M.; Di Rocco, G.; Hickey, N.; Geremia, S. High-resolution crystal structure of the recombinant diheme cytochrome c from Shewanella baltica (OS155). *J. Biomol Struct Dyn.* **2015**, 33(2), 395-403.

[32] DeLano, W.L. **2002**. The PyMOL Molecular Graphics System. Delano Scientific, San Carlos.

[33] Scheuermann, T.H.; Brautigam, C.A. High-precision, automated integration of multiple isothermal titration calorimetric thermograms: new features of NITPIC. *Methods.* **2015**, 76, 87-98.

[34] Zhao, H.; Piszczek, G.; Schuck, P. SEDPHAT--a platform for global ITC analysis and global multi-method analysis of molecular interactions. *Methods.* **2015**, 76, 137-148.

[35] Spinello, A.; Borišek, J.; Malcovati, L.; Magistrato, A. Investigating the Molecular Mechanism of H3B-8800: A Splicing Modulator Inducing Preferential Lethality in Spliceosome-Mutant Cancers. *Int J Mol Sci.* **2021**, 22(20), 11222.

[36] Anandakrishnan, R.; Aguilar, B.; Onufriev, A.V. H++ 3.0: automating pK prediction and the preparation of biomolecular structures for atomistic molecular modeling and simulations. *Nucleic Acids Res.* **2012**, 40, W537-41.

[37] Lindorff-Larsen, K.; Piana, S.; Palmo, K.; Maragakis, P.; Klepeis, J.L.; Dror, R.O.; Shaw, D.E. Improved side-chain torsion potentials for the Amber ff99SB protein force field. *Proteins.* **2010**, 78(8), 1950-8.

[38] Wang, J.; Wolf, R.M.; Caldwell, J.W.; Kollman, P.A.; Case, D.A. Development and testing of a general amber force field. *J Comput Chem.* **2004**, 25(9), 1157-74.

[39] Wang, J.; Wang, W.; Kollman, P.A.; Case, D.A. Automatic atom type and bond type perception in molecular mechanical calculations. *J Mol Graph Model.* **2006**, 25(2), 247-60.

[40] Van Der Spoel, D.; Lindahl, E.; Hess, B.; Groenhof, G.; Mark, A.E.; Berendsen, H.J. GROMACS: fast, flexible, and free. *J Comput Chem.* **2005**, 26(16), 1701-18.

[41] Bussi, G.; Donadio, D.; Parrinello, M. Canonical sampling through velocity rescaling. *J Chem Phys.* **2007**, 126(1), 014101.

[42] Miller, B.R.3rd; McGee, T.D.Jr.; Swails, J.M.; Homeyer, N.; Gohlke, H.; Roitberg, A.E. MMPBSA.py: An Efficient Program for End-State Free Energy Calculations. *J Chem Theory Comput.* **2012**, 8(9), 3314-21.

[43] Nguyen, H.; Roe, D.R.; Simmerling, C. Improved Generalized Born Solvent Model Parameters for Protein Simulations. *J Chem Theory Comput.* 2013, 9(4), 2020-2034.

[44] Borišek, J.; Saltalamacchia, A.; Spinello, A.; Magistrato, A. Exploiting Cryo-EM Structural Information and All-Atom Simulations To Decrypt the Molecular Mechanism of Splicing Modulators. *J Chem Inf Model.* **2020**, 60(5), 2510-2521.

[45] Humphrey, W.; Dalke, A.; Schulten, K. VMD: visual molecular dynamics. *J Mol Graph.* **1996**, 14(1), 33-8.

[46] Ayoub, A.T.; Craddock, T.J.A.; Klobukowski, M.; Tuszynski, J. Analysis of the strength of interfacial hydrogen bonds between tubulin dimers using quantum theory of atoms in molecules. *Biophys J.* **2014**, 107(3), 740-750.

[47] Hytönen, V.P.; Hörhä, J.; Airenne, T.T.; Niskanen, E.A.; Helttunen, K.J.; Johnson, M.S.; Salminen, T.A.; Kulomaa, M.S.; Nordlund, H.R. Controlling quaternary structure assembly: subunit interface engineering and crystal structure of dual chain avidin. *J Mol Biol.* **2006**, 359(5), 1352-63.

[48] Freitag, S.; Le Trong, I.; Klumb, L.; Stayton, P.S.; Stenkamp, R.E. Structural studies of the streptavidin binding loop. *Protein Sci.* **1997**, 6(6), 1157-66.

[49] Izrailev, S.; Stepaniants, S.; Balsera, M.; Oono, Y.; Schulten, K. Molecular dynamics study of unbinding of the avidin-biotin complex. *Biophys J.* **1997**, 72(4), 1568-81.

[50] Błauż, A.; Rychlik, B.; Makal, A.; Szulc, K.; Strzelczyk, P.; Bujacz, G.; Zakrzewski, J.; Woźniak, K.; Plażuk, D. Ferrocene-Biotin Conjugates: Synthesis, Structure, Cytotoxic Activity and Interaction with Avidin. *Chempluschem.* **2016**, 81(11), 1191-1201.

[51] Barker, K.D.; Eckermann, A.L.; Sazinsky, M.H.; Hartings, M.R.; Abajian, C.; Georganopoulou, D.; Ratner, M.A.; Rosenzweig, A.C.; Meade, T.J. Protein binding and the electronic properties of iron(II) complexes: an electrochemical and optical investigation of outer sphere effects. *Bioconjug Chem.* **2009**, 20(10), 1930-9.

[52] Plażuk, P.; Zakrzewski, J.; Salmain, M.; Błauż, A.; Rychlik, B.; Strzelczyk, P.; Bujacz, A.; Bujacz, G. Ferrocene−Biotin Conjugates Targeting Cancer Cells: Synthesis, Interaction with Avidin, Cytotoxic Properties and the Crystal Structure of the Complex of Avidin with a Biotin−Linker−Ferrocene Conjugate. *Organometallics*. **2013**, 32(20), 5774–5783.

[53] Tong, Y.; Mei, Y.; Li, Y.L.; Ji, C.G.; Zhang, J.Z. Electrostatic polarization makes a substantial contribution to the free energy of avidin-biotin binding. *J Am Chem Soc.* **2010**, 132(14), 5137-42.

Tables and Figures

Table 1. Data collection and refinement statistics. $R_{merge} = \sum | I - \langle I \rangle | / \sum I$ and $R_{work} = \sum | F_o - F_c | / \sum F_o$ with I intensity, F_o observed and F_c calculated structure factors.

PDB: 8CK7	
Scaling statistics	
Wavelength (Å)	1.0
Space group	P64
Cell dimensions (Å, º)	a=b=108.91 c=43.35 γ=120
Resolution (Å)	27.5 - 2.2 *(2.27 - 2.20)*
R_{merge}	0.146 *(0.376)*
No. observations	107219 *(5928)*
No. unique reflections	15151 *(1308)*
Mean ((I) / Sigma(I))	8.9 *(3.3)*
CC (1/2)	0.98 *(0.81)*
Completeness (%)	99.9 *(99.7)*
Redundancy	7.1 *(4.5)*
Refinement statistics	
Resolution (Å)	27.5 - 2.2
No. used reflections	14409
R_{work} / R_{free}	0.18 / 0.23
Protein Atoms/ B-factors ($Å^2$)	1864 / 20
Ligand Atoms/ B-factors ($Å^2$)	52 / 33.4
Solvent Atoms/ B-factors ($Å^2$)	103 / 24.3
Ramachandran	97.4% favoured 2.6% allowed

Table 2. Binding free energies. Overall binding free energy (ΔG_b, kcal/mol) of avidin-TEP, avidin-GUA and avidin-BIO complexes are reported together with their per-residue decomposition analysis of MD trajectories obtained using the Molecular Mechanics Generalized Surface Area method (MM-PBSA). Residues stabilizing the binding pose are marked in yellow (ΔG_b smaller than -1.0 kcal mol), light green (ΔG_b between -1.01 and -2.00 kcal/mol) and dark green (ΔG_b greater than -2.01 kcal/mol).

		Theophylline TEP	**8-oxodeoxyguanosine GUA**	**Biotin BIO**
ΔG_b complex		*-9.67 ± 0.27*	*- 10.14 ± 0.29*	*-22.02 ± 0.30*
ΔG_b per-residue	Leu14	-0.37 ± 0.03	-1.00 ± 0.07	-1.23 ± 0.02
	Ser16	-	-0.20 ± 0.03	-2.98 ± 0.05
	Tyr33	-0.57 ± 0.10	-0.09 ± 0.07	-3.24 ± 0.06
	Thr35	-0.43 ± 0.04	-0.18 ± 0.02	-2.52 ± 0.05
	Val37	-1.16 ± 0.07	-0.12 ± 0.02	-1.18 ± 0.03
	Thr38	-2.22 ± 0.10	-0.56 ± 0.05	-4.79 ± 0.12
	Ala39	-0.39 ± 0.03	-	-1.65 ± 0.09
	Trp70	-0.34 ± 0.02	-1.57 ± 0.06	-1.57 ± 0.06
	Ser73	-	-	-2.28 ± 0.03
	Ser75	-	-	-2.48 ± 0.12
	Thr77	-0.37 ± 0.02	-2.33 ± 0.07	-1.27 ± 0.05
	Trp97	-2.98 ± 0.06	-4.02 ± 0.09	-1.77 ± 0.02
	Leu99	-0.66 ± 0.02	-1.32 ± 0.03	-1.94 ± 0.03

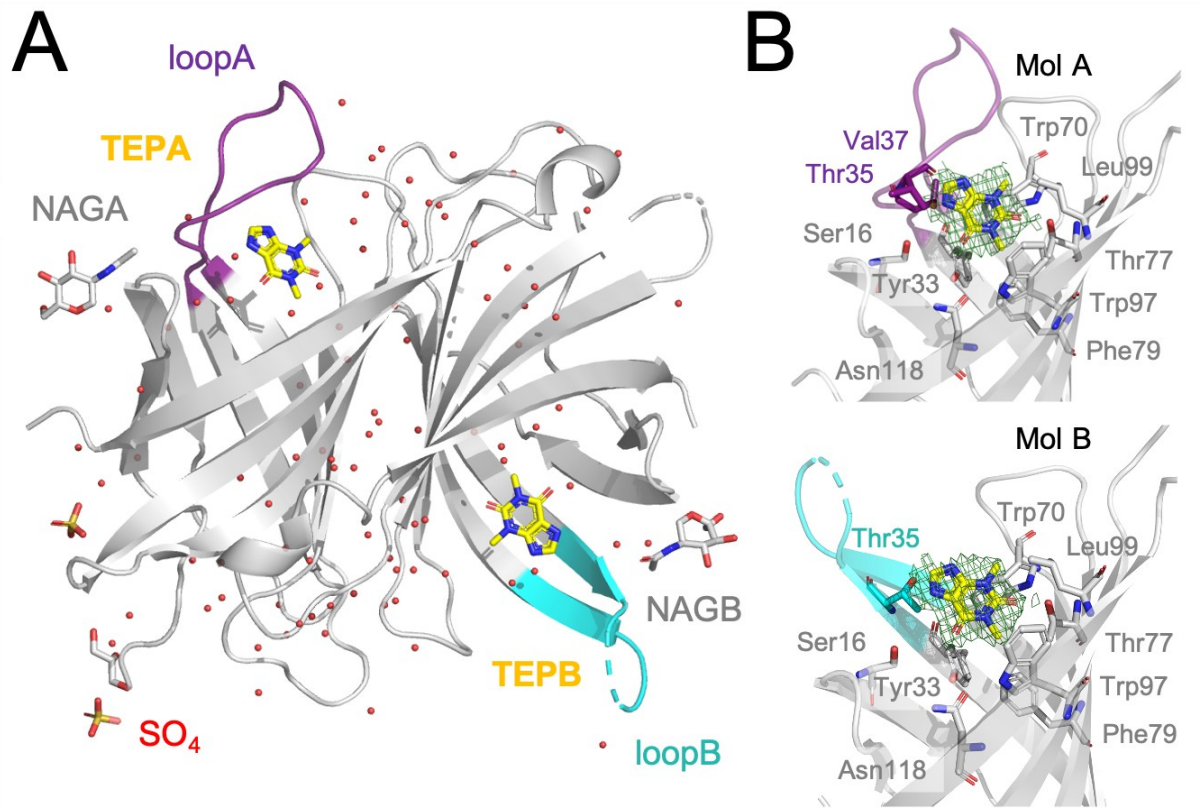

Figure 1. Crystal structure of avidin-TEP complex. (A) Overall structure of avidin (white, cartoon) in the dimeric form with TEP molecules (sticks, yellow), the flexible loop (loopA closed, magenta; loopB opened, cyan), waters (non-bonded spheres) and solvent (NAG and SO_4). (B) TEP interaction pattern (residues, sticks) in the avidin binding pocket. Colours refer to panel A. The unbiased difference Fo-Fc electron density map contoured at 3σ around TEP is shown as green mesh.

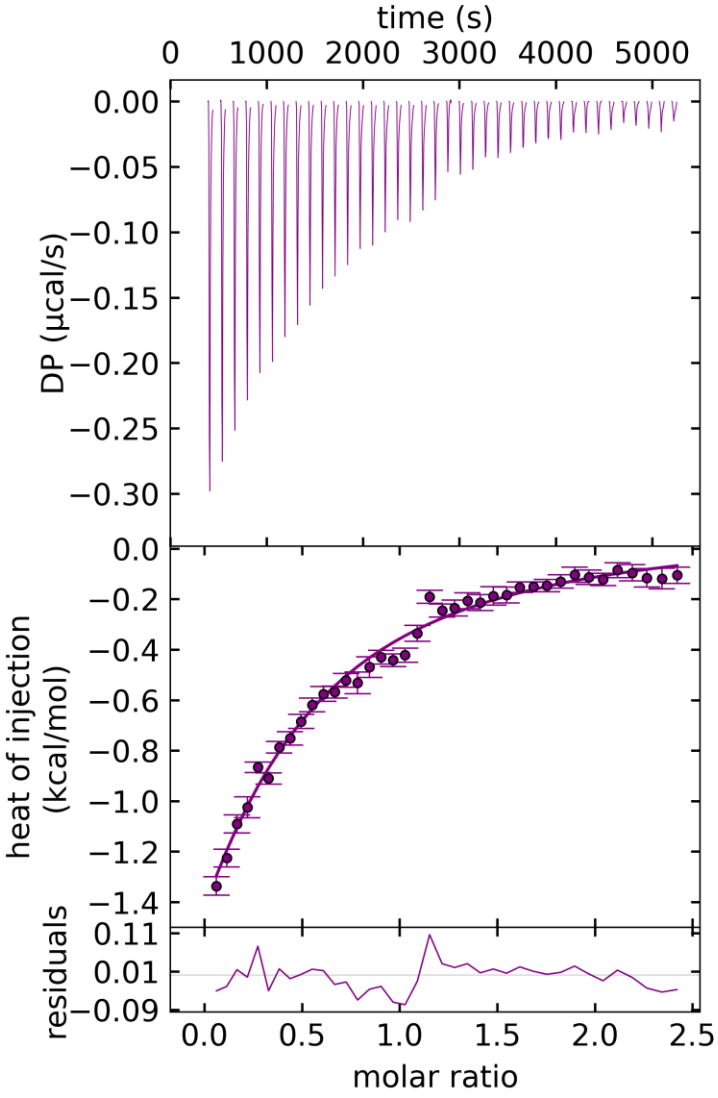

Figure 2. ITC analysis of avidin-TEP complex. ITC thermogram registered at 25 °C after addition of TEP 1.62 mM to a solution of avidin 330 µM dissolved in PBS at pH 7.4 is shown in the upper panel. The integration and fit of the points, represented with standard deviation are shown in the lower panel.

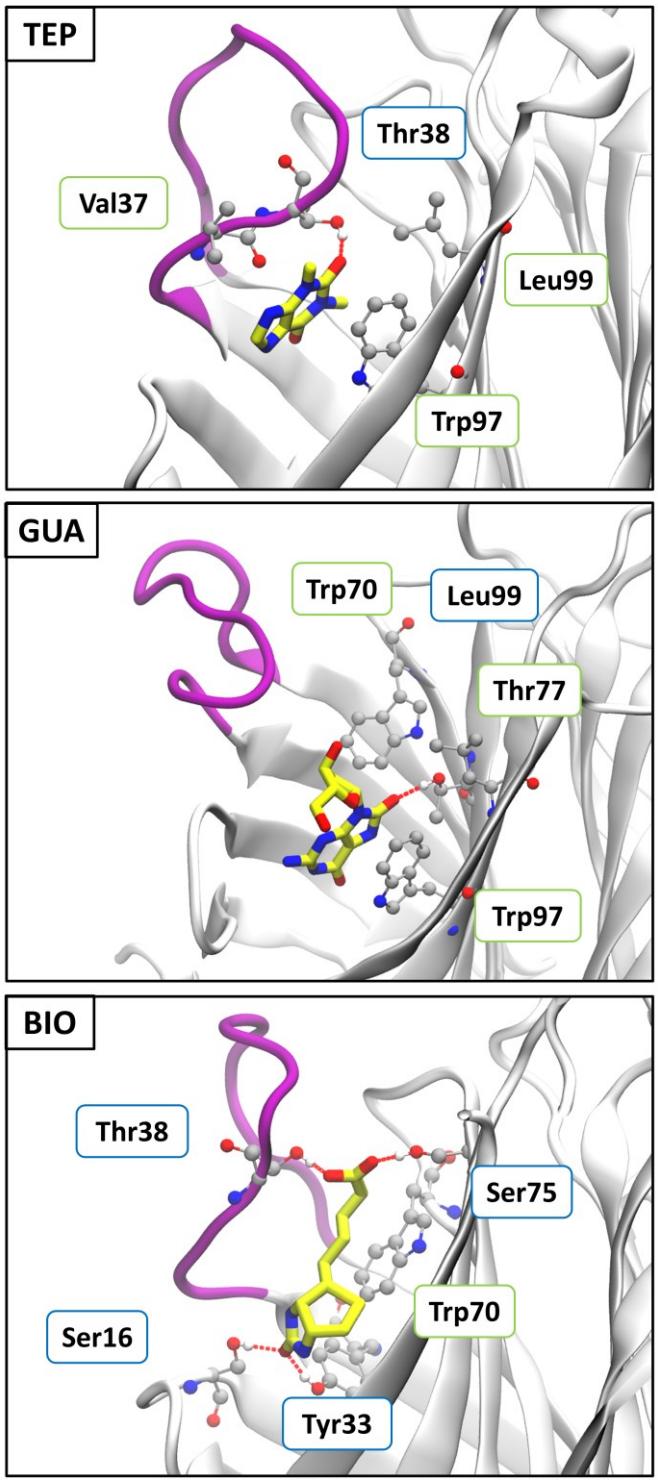

Figure 3. MD simulations. Representative binding poses for the avidin-TEP, avidin-BIO and avidin-GUA complexes as extracted from MD trajectories. Avidin monomers are displayed in silver new cartoons, the binders are shown in yellow sticks. Residues mostly contributing to the binding are shown in balls and sticks and among these, those forming hydrophobic and electrostatic interactions are highlighted and squared in green and blue, respectively. Hydrogen bonds are displayed as dashed lines red.